JACS
JOURNAL OF THE AMERICAN CHEMICAL SOCIETY

Article

pubs.acs.org/JACS

On the Accessibility to Conical Intersections in Purines: Hypoxanthine and its Singly Protonated and Deprotonated Forms

Juan. P. Villabona-Monsalve,[†] Raquel Noria,[†] Spiridoula Matsika,[‡] and Jorge Peón*,[†]

[†]Instituto de Química, Universidad Nacional Autónoma de México, Circuito Exterior, Ciudad Universitaria, México, 04510, D.F., México

[‡]Department of Chemistry, Temple University, 13th and Norris Streets, Philadelphia Pennsylvania 19122, United States

ABSTRACT: The dynamics following electronic excitation of hypoxanthine and its nucleoside inosine were studied by femtosecond fluorescence up-conversion. Our objective was to explore variants of the purinic DNA bases in order to determine the molecular parameters that increase or reduce the accessibility to ground state conical intersections. From experiments in water and methanol solution we conclude that both dominant neutral tautomers of hypoxanthine exhibit ultrashort excited state lifetimes (τ < 0.2 ps), which are significantly shorter than in the related nucleobase guanine. This points to a more accessible conical intersection for the fluorescent state upon removal of the amino group, present in guanine but absent in hypoxanthine. The excited state dynamics of singly protonated hypoxanthine were also studied, showing biexponential decays with a 1.1 ps component (5%) besides a sub-0.2 ps ultrafast component. On the other hand, the S_1 lifetimes of the singly deprotonated forms of hypoxanthine and inosine show drastic differences, where the latter remains ultrafast but the singly deprotonated hypoxanthine shows a much longer lifetime of 19 ps. This significant variation is related to the different deprotonation sites in hypoxanthine versus inosine, which gives rise to significantly different resonance structures. In our study we also include multireference perturbation theory (MRMP2) excited state calculations in order to determine the nature of the initial electronic excitation in our experiments and clarify the ordering of the states in the singlet manifold at the ground state geometry. In addition, we performed multireference configuration interaction calculations (MR-CIS) that identify the presence of low-lying conical intersections for both prominent neutral tautomers of hypoxanthine. In both cases, the surface crossings occur at geometries reached by out of plane opposite motions of C2 and N3. The study of this simpler purine gives several insights into how small structural modifications, including amino substitution and protonation site and state, determine the accessibility to conical intersections in this kind of heterocycles.

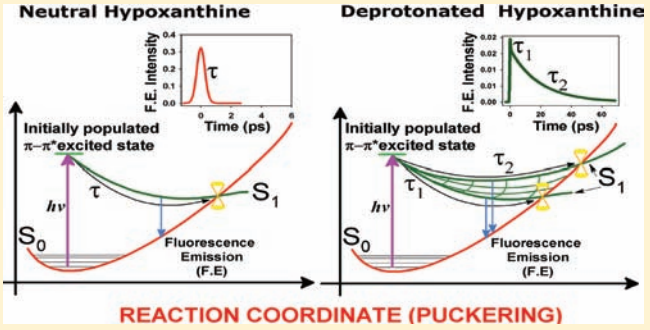

INTRODUCTION

Ultrashort excited state lifetimes (τ < 1 ps) and extremely low fluorescence quantum yields ($\sim 10^{-4}$) are the main photophysical characteristics of the purinic DNA bases.[1−4] The efficient elimination of electronic energy in these systems is likely to have been a key element in the early stages of the molecular evolution which determined the basic elements of the genetic material.[5] These systems are also among the most important prototypes to study ultrafast evolution in electronically excited states and nonadiabatic processes since the wavepacket motions result in rapid and highly efficient changes in the electronic states.[6−8]

The subpicosecond excited state decays observed in these molecules come from crossings between the potential energy surfaces in the low lying electronic states. Over the past few years, it has come into view that these conical intersections (CIs), in fact play a central role in several ultrafast processes of primary relevance in photochemistry.[2−5,9,10] High level computational methods (e.g., CASSCF/CASPT2) have shed light into the intrinsic reaction coordinates which ensure the accessibility to a CI. Together with experimental work with femtosecond resolution, the calculations have started to give detailed information on the relations between the molecular structure and the excited state decay dynamics.[11,12] Several issues however remain open for a full description, including questions about the basic elements in a molecular framework which guarantee the presence of an accessible CI, and how small modifications in the molecular structure affect such accessibility.

In this contribution we present fluorescence up-conversion experiments which explore the evolution of the emissive states in a variant of purinic DNA bases. Our aim was to observe how discrete changes in a molecule produce effects on the fluorescence lifetimes, and from this, deduce factors that influence the accessibility to CIs. We have focused on the most prominent tautomers of hypoxanthine (HPX) and its nucleoside inosine (INS). The compounds of our study can be

Received: January 17, 2012
Published: April 9, 2012

dx.doi.org/10.1021/ja300546x | J. Am. Chem. Soc. 2012, 134, 7820−7829

considered as variants of guanine and guanosine respectively, as shown in Figure 1. Specifically, we were interested in how the

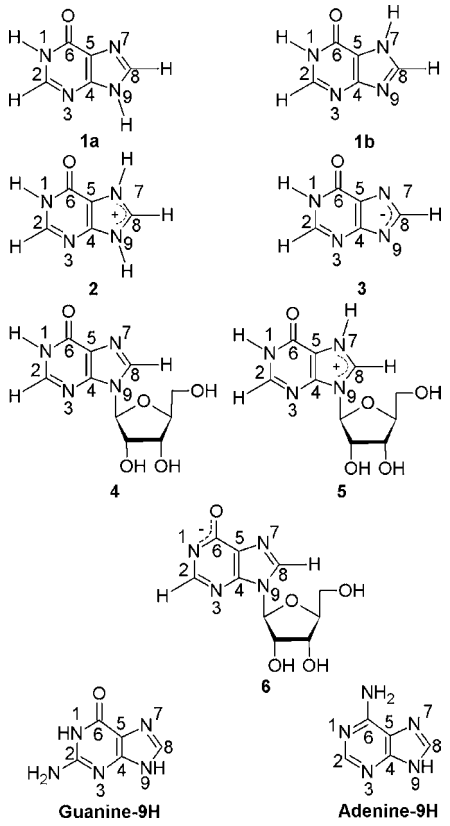

Figure 1. Predominant tautomers of hypoxanthine (HPX) and inosine (INS) at different pH values in aqueous solution: (1a) keto-N9-H HPX tautomeric form, present in pH = 5 aqueous solution; (1b) keto-N7-H HPX tautomeric form, present in pH = 5 aqueous solution; (2) singly protonated form of HPX, predominant in pH = 1 aqueous solution; (3) singly deprotonated form of HPX, predominant in pH = 10 aqueous solution; (4) INS neutral form in pH = 6 aqueous solution; (5) singly protonated INS, predominant in an HCl 1 N aqueous solution; (6) singly deprotonated INS, predominant species in pH = 10 aqueous solution.

removal of the amino group in guanine (to yield hypoxanthine) changes the fluorescent state decay.

We are also interested in studying how the protonation state of these molecules affects the excited state dynamics. Changing the degree of protonation of the purines changes not only the substitution pattern, but also, the molecular orbital description of the system. This has triggered interest in the protonated forms of some nucleic acid bases. Most noteworthy are the studies of singly protonated guanine, guanosine and GMP which have shown that upon protonation at site N7, the S_1 lifetime becomes longer by a factor of more than 100.[13,14] Such results have been well described by TD-DFT calculations which have shown differences in the shape of the S_1 surface which changes the accessibility to a ground state CI in comparison with the neutral compound (also see Results and Discussion Section).[13] On the other hand, gas phase studies of monoprotonated adenine have demonstrated that in this case, the excited state decay does not vary drastically with respect to the neutral 9-H tautomer.[15] Excited state calculations have shown that for this base, single protonation (to yield 1-H,9-H adenine$^+$, the most stable tautomer in gas phase) is associated with the presence of a similar CI (through an out-of-plane coordinate) to the one in adenine (9-H).[16]

In this contribution, we have studied how both protonation and deprotonation modify the dynamics of neutral HPX and INS. For these systems, protonation of HPX and INS produce analogous structures (with hydrogen atoms bonded to N7 and N9), but single deprotonation occurs at different sites producing two different kinds of aromatic systems (see deprotonated species in Figure 1 and below). As far as we know, this is the first study of monoanionic species of this type, which are accessible in HPX and INS thanks to the fact that the first and second deprotonation pK_a values are sufficiently different to have a vast population majority of the singly deprotonated forms at specific pHs.

A sketch of the excited state deactivation process in terms of the different effects on the potential energy surfaces can in principle be inferred from the present fluorescence up-conversion experiments together with theoretical studies. In this contribution we include high level computational studies of the low lying electronically excited states at the ground state geometry in order to determine the type of electronic states accessed by light absorption in the region of the first absorption bands, as well as the nature of the state detected by time-resolved fluorescence. As will be shown this is particularly relevant for the keto−N7-H tautomer and the ionized forms which are hereby addressed for the first time experimentally and computationally. We also include calculations at the multireference configuration interaction level (MR-CIS), which isolate the relevant S_1−S_0 crossing regions for the most important tautomers of HPX: the keto−N9-H, and the keto−N7-H species. The calculations show the presence of low-energy, highly accessible CIs for both these tautomers. The theoretical studies for the ionized forms will be presented in a separate contribution.

METHODS

Experimental Section. HPX (>99%), INS (>99%), and IMP (>99%) were purchased from Sigma-Aldrich and were used without further purification. Aqueous solutions were prepared dissolving the compounds in ultrapure deionized water obtained from a MILLIPORE (Milli-Q) system. The pH of the solutions was adjusted with very high purity NaOH 0.1 M or HCl 1 M aqueous standard solutions, also acquired from Aldrich. Solute concentrations were adjusted to give an absorbance of approximately 1 in a 1 mm path length quartz cell at the excitation wavelength of 257 nm. Absorption spectra were obtained in a 1 cm or 1 mm quartz cell with a Cary-50 spectrophotometer (Varian). Steady-state fluorescence spectra were measured in a 1 cm quartz cell with a Cary-Eclipse fluorimeter (Varian). In the up-conversion experiment,[17] about 150 mL of solution were flown through a quartz cell (1 mm path length with 1 mm windows), and was excited with the third harmonic pulses (λ = 257 nm) from a Ti:Sapphire regenerative amplifier (Legend-F, Coherent) with a repetition rate of 1 kHz. The 770 nm seed pulses were obtained from a Ti:Sapphire oscillator (NJA-5, Clark MRX Corporation, repetition rate: 100 MHz). Fluorescence from the sample was collected by two parabolic mirrors and focused in a type I β-BBO crystal where it was crossed with a 770 nm gate pulse to obtain an up-converted signal. The sum-frequency mixing light was focused into a double 10 cm monochromator (ORIEL) and detected by a photomultiplier tube.[18] In all cases, it was verified that the up-conversion signals were absent in blank solutions with the same HCl or NaOH concentrations in back-to-back experiments. All traces were fitted to exponential functions convoluted with the Instrumental Response Function (IRF). This function was considered to be Gaussian with a full width at half-maximum of 550 fs, as determined through nonlinear least-squares fits to fluorescence up-conversion

dx.doi.org/10.1021/ja300546x | J. Am. Chem. Soc. 2012, 134, 7820−7829

measurements on *p*-terphenyl in cyclohexane solution at the same wavelength of 350 nm. For the IRF measurement, the instrumental response was taken as an adjustable parameter given that the *p*-terphenyl signal evolution times are much slower than the instrumental response at this wavelength.[19]

It is possible that in aqueous solutions, purine type systems may self-associate.[20−24] This can favor the occurrence of excited state deactivation processes related to the presence of aggregates, including energy transfer, electron transfer, and proton transfer. To rule out these effects, fluorescence up-conversion measurements were checked for concentrations from 0.25 to 2.8 mM. This covers an order of magnitude in concentration, and showed that the decay behavior does not change. To obtain the working absorbance, the concentration was around 2 mM depending on the system. It should also be noted that for the concentration range of our experiments, no association effects on the spectroscopy have been observed in guanine and adenine which are analogous to HPX.[4,14,25] The pH measurements were done with a high sensitivity digital pH-meter which allows measurements of pH as low as near zero (Orion Research Inc., Ag/AgCl internal reference electrode). All experiments were performed at room temperature (20 ± 0.5 °C).

Computational Methods for the Vertical Transitions at the Ground State Geometry. Geometry optimizations for the electronic ground state were done at the MP2 level of theory and constrained to the *Cs* symmetry, using the double-ζ plus polarization (cc-pvdz) Gaussian basis set of Dunning. Vertical excitation energies and oscillator strengths were computed at the state averaged complete active space self-consistent field (SA-CASSCF) level using an active space of 18 electrons in 13 active molecular orbitals (18,13) with the 6-31G+(d) basis set. Four singlet A′ states (ground state and three excited states) and four singlet A″ excited states were state averaged. Excitation energies were corrected at the multireference perturbation theory MRMP2 level.[26,27] For all the systems the active space includes three molecular orbitals from the lone pairs (one for the oxygen atom and two for the nitrogen atoms) and 10 π molecular orbitals. These high-level multireference methods have been used extensively for the study of excited states of purinic DNA bases.[6,28−30] The calculations were carried out using the GAMESS quantum package,[31] and the graphical user interface Macmolplt was used for the molecular orbital visualization.[32]

Conical Intersections Calculations. Energies were computed at the multireference configuration interaction with single excitations (MR-CIS) level using as reference a complete active space. The molecular orbitals were obtained from a SA-CASSCF calculation using a complete active space (CAS) of 12 electrons in nine active orbitals (12, 9). The cc-pvdz basis set of Dunning was used. The subsequent MR-CIS calculation used the same CAS and included only single excitations to the virtual space. From an initial excited state analysis, four states were averaged (ground state, two $\pi-\pi^*$ states, and one $n-\pi^*$ state). The excitation energy computations ($S_1 \leftarrow S_0$) at the MR-CIS/SA-CASSCF(12,9)/cc-pvdz level of theory include less correlation than the MRMP2/SA-CASSCF(18,13)/6-31G+(d) level, however, this reduction on the level of theory has been seen to be appropriate and without systematic errors for the geometry optimization of the excited state and the conical intersection search.[7] The MR-CIS excitation energies in this work were also compared to the MRMP2 to ensure that there is no change on the ordering of states, which could change the results even qualitatively.

Minima on the crossing seam (MXS) for the conical intersections were computed by a restricted gradient algorithm using the analytical derivatives of the MR-CIS wave function as implemented in the COLUMBUS quantum chemistry package.[33,34] This methodology has been proved to be adequate for the conical intersection optimization on DNA bases.[6,35−37] Energies at the MXS geometry found with the MR-CIS level of theory were recalculated at the MRMP2 level by using the orbitals from a SA-CASSCF(18,13) computation so that dynamical correlation will be included more adequately. Six states were averaged and the 6-31G+(d) basis set was used in this recalculation.

RESULTS AND DISCUSSION

First, we give an overview of the chemical equilibria important for these systems: HPX global pK_a values are: 2.04, 8.64 and 11.5.[38] With these pK_a values, in a pH = 1 HPX aqueous solution, the monoprotonated species predominates (≈ 92%). A pH of 10 HPX aqueous solution maximizes the population of singly deprotonated species (∼93%), and in a pH = 5 HPX aqueous solution, the neutral species predominates (>98%). For INS, the pK_a values have been reported to be: 0.97, 8.50, and 11.65.[39,40] For this case, in order to study the singly protonated specie, the molecule was dissolved in high purity 1 N HCl solution (monoprotonated form: 90% with the rest as the neutral species, pH ∼0). The neutral specie of INS was studied in pH = 6 aqueous solution, while for the singly deprotonated INS species, the pH was adjusted to 10 (mole fraction = 95%).

In Figure 1 we show the molecular structures of the dominant tautomers of HPX and INS at the different pH values. The relevant tautomers in solution phase have been established in the literature according to Raman, UV−vis, and NMR (^{13}C and ^{1}H) spectroscopy, and theoretical studies.[38,39,41−51] For neutral HPX, it is accepted that the keto−N9-H tautomeric form (**1a** in Figure 1) is the dominant tautomer in aqueous solution. However, the keto−N7-H **1b** tautomeric form is also considered to be present in significant concentration in aqueous solution, although there are no precise measurements for the relative populations.[43,46,47,52,53]

From NMR studies, the mol fraction of the HPX keto-N7-H tautomer in D_4-methanol at 204 K is known to be 54%, with the rest corresponding to the keto-N9-H tautomer. At 303 K, these percentages correspond to 53% and 47% respectively,[54] while in room temperature DMSO, the relative concentrations of keto-N7-H and keto-N9-H are 58% and 42% respectively.[47] As will be shown, from experiments in water and in methanol, we will be able to ascertain the ultrafast photophysics of both tautomers despite the uncertainty in their relative populations in water. The aforementioned pK_a values and tautomer studies allowed establishing the relevant singly protonated and singly deprotonated species at low (pH ≤ 1) and high pH (pH = 10).[39,44] The respective structures are included in Figure 1.

Steady State Results and Computational Results at the Ground State Geometry. Figure 2 shows the steady state absorption spectra of HPX and INS. As can be seen, the pH = 5 HPX and methanolic systems show a single band centered on 250 nm. The neutral INS solutions on the other hand show some structure in this first band, with a tail or shoulder appearing in the region of 260 to 290 nm besides the maximum centered at 249 nm. This feature is similar to that of 9-methylhypoxanthine as reported by Tinoco et al., and has been related to the presence of two bright electronic transitions in this zone, one predominant in the 259−277 nm zone, and one at 249 nm in water at pH = 6.1.[45] For the case of HPX aqueous solutions, it is most likely that the single band we observe is also made of the superposition of two states (for both tautomers) as described previously,[49,55] which is in accord with our theoretical calculations (see next).

Our MRMP2 calculations for the gas phase vertical transitions are summarized in Tables 1 and 2. These results confirm that both dominant tautomers of neutral HPX (keto-N9-H and keto-N7-H) have two low lying transitions with significant oscillator strength which should make up the band centered at 250 nm in aqueous solution. This is to our

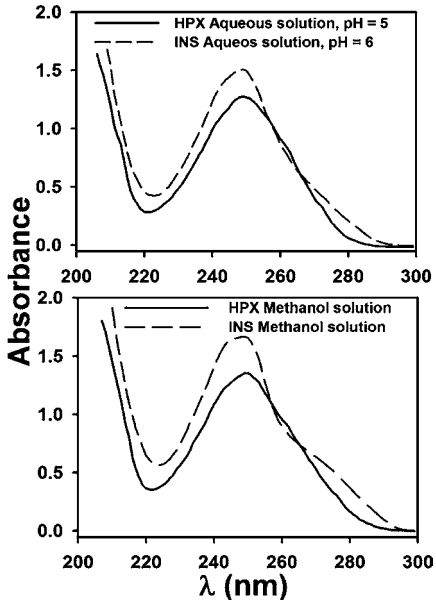

Figure 2. Top: Steady state absorption spectra of hypoxanthine (HPX) and inosine (INS) in neutral aqueous solution. Bottom: Steady state absorption spectrum of HPX in methanol solution.

knowledge, the first excited state ab initio high level calculation for the keto-N7-H tautomer, the singly protonated specie (HPX^+) and a singly deprotonated purine base (HPX^-). As will be shown, these calculations are essential when assessing the photophysics observed for the HPX/methanol solution since in this solvent, both tautomers are known to be present in approximately the same proportion. According to the analysis in Table 2, the ^1L_a type state is the first electronically excited state for both neutral tautomers. In this sense, the MRMP2 calculations of Table 1 are in good accordance with previous calculations using the TD-DFT and TD-DFT/PCM methodologies which have shown that two $\pi-\pi^*$ states contribute to the first absorption band (composite band as mentioned in the previous paragraph).[49,56] Besides these $\pi-\pi^*$ transitions, our MRMP2 calculations indicate the presence of three dark $n-\pi^*$ transitions above the first $\pi-\pi^*$ state. As has been established for adenine and guanine, the $n-\pi^*$ states are expected to be significantly destabilized in aqueous solution in comparison with the gas phase due to the specific hydrogen bonding type interactions with the solvent.[13,57]

The calculations at the same level of theory for the singly protonated and singly deprotonated forms of HPX reveal that in both cases, there are also two bright, $\pi-\pi^*$ transitions in the region of the first electronic band (see Tables 1 and 2). For

Table 2. Contributions of Configuration State Functions (CSF) in the 2 $^1A'$ and 3 $^1A'$ Excited States of Hypoxanthine (HPX, keto-N9-H and keto-N7-H Tautomers), Singly Protonated (HPX^+), and Singly Deprotonated (HPX^-) Hypoxanthine[a]

system	CSF	2 $^1A'$ (%)[b]		3 $^1A'$ (%)	
keto-N9-H	H → L	62	(115)	2.6	(54)
	H → L +1	3.3		36	
	H − 1 → L	0.4		29	
	H − 2 → L	2.6		1.2	
keto-N7-H	H → L	58	(−19)	2.5	(17)
	H → L +1	6.2		35	
	H − 1 → L	0.5		24	
	H − 2 → L	2.3		1.0	
HPX^+	H → L	48	(5)	19	(79)
	H → L +1	15		44	
	H − 1 → L	<0.1		3.1	
	H − 2 → L	0.3		<0.1	
HPX^-	H → L	80	(133)	0.4	(24)
	H → L +1	<0.1		42	
	H − 1 → L	0.6		24	
	H − 2 → L	1.0		0.9	

[a]Values in parentheses are the transition dipole moment directions (Φ) in degrees, according to the Tinoco DeVoe convention shown below.[44] [b]Percentages are the squares of the coefficients taken from the CASSCF wave functions.

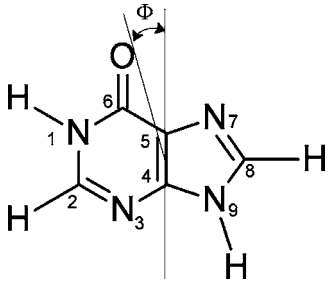

both HPX^+ and HPX^-, the lowest energy $\pi-\pi^*$ transition is of ^1L_a type and has an oscillator strength of about 25% that of the next electronic $\pi-\pi^*$ state, of ^1L_b type. For HPX^- our MRMP2 calculations predicts that there are two dark $n-\pi^*$ states near the optically accessed ^1L_a ($\pi-\pi^*$) excited state. Again, similarly to the neutral tautomers, it is most likely that the first band (at about 250 nm for HPX^+ and 260 nm for HPX^-) is a composite with the ^1L_a state as the first bright singlet excited state. In summary, the first $\pi-\pi^*$ singlet excited states for all the systems of our study have been calculated as primarily HOMO→LUMO excitations (^1L_a), but the 250 nm 260 nm region is considered to be a band composed of the two lowest

Table 1. Vertical Excitation Energies (eV) at the MRMP2 Level and Oscillator Strengths at the CASSCF Level for the First Three A′ and A″ Excited States of Hypoxanthine (HPX, keto-N9-H and keto-N7-H Tautomers), Singly Protonated Hypoxanthine (HPX^+) and Singly Deprotonated Hypoxanthine (HPX^-)[ab]

system	2 $^1A'$	3 $^1A'$	4 $^1A'$	1 $^1A''$	2 $^1A''$	3 $^1A''$
keto-N9-H	4.485 (0.146)	5.442 (0.029)	6.103 (0.001)	5.252	5.282	5.446
keto-N7-H	4.637 (0.101)	5.252 (0.026)	6.225 (0.192)	4.876	5.146	6.056
HPX^+	4.520 (0.049)	4.678 (0.244)	5.927 (0.001)	4.616	5.334	5.756
HPX^-	5.039 (0.031)	5.222 (0.123)	5.609 (0.024)	4.910	4.915	5.057

[a]For 9-methyl-hypoxanthine the reported experimental vertical transitions are 4.41 eV, 5.18 eV, 6.04 and 6.42 eV for the vapor phase, and 4.59 4.77 eV, 4.98 and 6.20 eV in aqueous solution at pH 6.1.[34] The HPX experimental values of the maximum on the absorption spectrum in neutral, acidic or basic aqueous solutions are: 4.98 eV (pH 5), 5.00 eV (pH 1) and 4.80 eV (pH 10), this work. [b]Oscillator strengths are indicated in parentheses.

dx.doi.org/10.1021/ja300546x | J. Am. Chem. Soc. 2012, 134, 7820−7829

energy $\pi-\pi^*$ transitions, which is similar to the situation in guanine.[44] It should be noted that the energy of ^1L_b is more sensitive to the protonation state compared to the energy of ^1L_a and so the gap between the two components also changes at different pH.

Excited State Dynamics. The third harmonic of our laser system (257 nm) produces a population of electronically excited molecules through light absorption near the center of the first UV-band for all the systems of this study. As mentioned previously, this band has been described as a composite of transitions for the first two bright states in the neutral HPX tautomers.[28,45,55,56,58] For the neutral HPX and INS solutions (pH = 5 and 6, respectively), it was not possible to obtain accurate steady state emission spectra, implying a fluorescence quantum yield of less than 10^{-4}. This is estimated from comparisons with the emission signal from anthracene solutions in methanol. The up-conversion experiments were set to detect 350 nm since this detection wavelength provided the largest signal in the time-resolved experiments for all the systems (see below). The fluorescence traces included in the insets of Figure 3 show that the faint steady state emissions

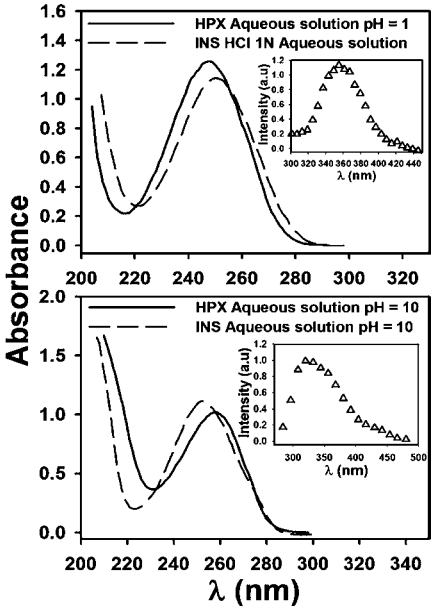

Figure 3. Top: Steady state absorption spectra of hypoxanthine (HPX) and inosine (INS) in acidic aqueous solution. Inset: HPX Fluorescence emission spectrum in pH = 1 solution (λ_{Exc} = 257 nm). Bottom: Steady state absorption spectra of HPX and INS in basic aqueous solution. Inset: HPX fluorescence emission spectrum in basic aqueous solution (λ_{Exc} = 250 nm).

from the ionized forms are localized in this spectral region and correspond to emission quantum yields of the order of 10^{-4}.

Photophysics of Neutral Hypoxanthine and Inosine. Figure 4a shows the 350 nm fluorescence decay of HPX in aqueous solutions at pH = 5. It should be noted that this pH is reached by the system at the working concentration without the addition of buffers, and that the neutral tautomers population corresponds to more than 98%. The emission shows an ultrafast decay which can be fitted by a single exponential function with a τ < 0.2 ps decay convoluted with the instrumental response function. All the previous and present theoretical calculations, including TD-DFT (with and without explicit solvent),[49,56] as well as multireference methods,[56] are

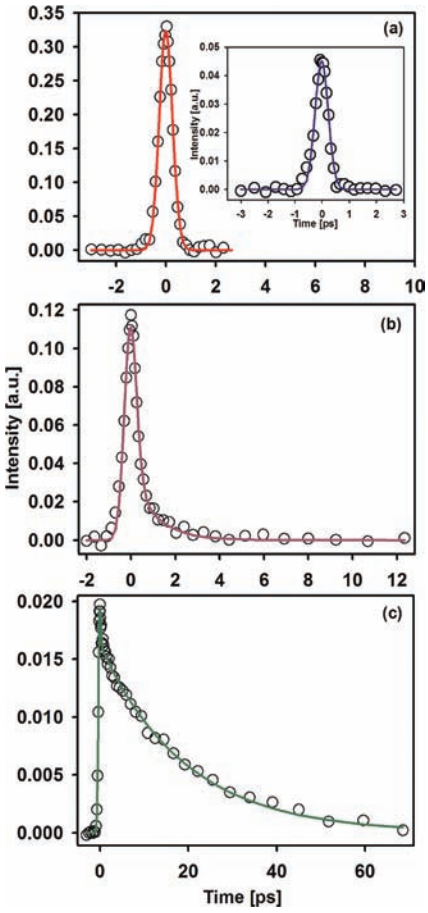

Figure 4. Fluorescence up-conversion measurements of hypoxanthine (HPX) in different aqueous solutions. (a) pH = 5. Inset fluorescence emission decay of hypoxanthine in methanol solution. (b) pH = 1. (c) pH = 10. In all cases the excitation and detection wavelength were 257 and 350 nm respectively. The solid lines are nonlinear least-squares fits to exponential decays convoluted with the instrument response function.

consistent in assigning the first excited state as a bright $\pi-\pi^*$ state (verified to be ^1L_a type, for both tautomers in our calculations). This implies that the emission detected in all the systems of this study corresponds to fluorescence from the emissive first singlet excited state. This also indicates nearly instantaneous $S_n \rightarrow S_1$ internal conversion processes populating the fluorescent S_1 state when the original excitation is produced at the composite band. The latter has been also well established for the parent compound guanine.[13,59] For HPX^-, it should be noted that our gas phase MRMP2 calculations indicate the presence of two $n-\pi^*$ states at nearly the same energy as the first $\pi-\pi^*$ state (^1L_a). For this system, it is assumed that similarly to other systems, the $n-\pi^*$ states are destabilized, in the aqueous media.

The ultrafast depopulation of the fluorescent S_1 state (τ < 0.2 ps) is indicative of a highly accessible conical intersection with the electronic ground state. Such assignment is consistent with recent transient absorption experiments which were reported during the course of this investigation.[60] Such result verified the subpicosecond repopulation of the electronic ground state in this system. Together with the present study, these results also show that HPX has an electronic deactivation channel comparable with the DNA base with the fastest S_1 decay: adenine (keto-N9-H tautomer).[61]

dx.doi.org/10.1021/ja300546x | J. Am. Chem. Soc. 2012, 134, 7820−7829

Given that it is likely that to some extent, both the keto-N9-H and keto-N7-H tautomers of HPX are present in aqueous solution at pH = 5, our measurements suggest that both species have ultrafast fluorescence decays. This statement is further demonstrated with the HPX fluorescence decay at 350 nm in methanol solution shown in the inset of Figure 4a. As mentioned previously, in this solvent at room temperature the tautomer populations (keto-N9-H and keto-N7-H) are approximately equal (53−54% for keto-N7-H). Since the methanolic HPX solutions also show a single exponential decay with τ < 0.2 ps, we can conclude that both tautomers have ultrashort lifetimes. It should be noted that according to the calculations mentioned in the previous section, the first transitions for both tautomers have comparable oscillator strengths (see Table 1). This implies that significant excited state populations are created for both tautomers, and that their time-resolved $S_1 \rightarrow S_0$ emissions are of comparable intensity (signal strength is determined by the radiative rate and the initial populations[4]). The nonlinear least-squares fitting parameters of the fluorescence decays for all the systems are summarized in Table 3.

Table 3. Curve Fitting Parameters for Up-Conversion Traces of HPX and INS Aqueous Solutions[a]

	pH	a_1	τ_1 [ps]	a_2	τ_2 [ps]
HPX	5	1	<0.2		
HPX	1	0.95	<0.2	0.05	1.1 ± 0.1
HPX	10	0.60	<0.2	0.40	19 ± 0.4
INS	6	1	<0.2		
INS	HCl 1N	0.88	0.39 ± 0.01	0.12	2.5 ± 0.01
INS	10	1	<0.2		

[a]Data was described by single (a_2 = 0) or double-exponential functions, $I(t) = a_1 \cdot \exp(-t/\tau_1) + a_2 \cdot \exp(-t/\tau_2)$ convoluted with the instrument response function (fwhm ≈ 550 fs). λ_{Exc} = 257 nm and λ_{Det} = 350 nm. The total amplitudes of the signals were normalized to one.

INS should exhibit similar photophysics to the keto-N9-H tautomer of HPX given that the N7 position is of iminic type in both molecules and that the nitrogen atom at position 9 is in both cases, sp^3 hybridized, with a σ bond to a hydrogen atom or the ribose moiety. Figure 5a shows the fluorescence emission decay at 350 nm for INS in aqueous solutions at pH = 6. The fluorescence decay is again ultrafast with a single decay of τ < 0.2 ps. This result is completely consistent with the ultrafast excited state decay of the tautomer keto-N9-H of HPX. The INS result confirms that the biologically relevant neutral purinic chromophore of these systems has an intrinsically ultrafast S_1 decay independent of whether N9 or N7 is of iminic type.

Calculations of the Conical Intersections for the Neutral Tautomers. Vertical excitation energies for the first $\pi-\pi^*$ excited state of HPX-keto-N7-H and HPX-keto-N9-H at the MR-CIS/SA-CASSCF(12,9)/cc-pvdz level of theory are shown in Table 4. Due to the different treatment of correlation, these energies are higher than those calculated at the MRMP2/SA-CASSCF(18,13)/6-31G+(d) level (see Table 1). Since the MR-CIS method has limited dynamical correlation it is expected that it will overestimate the excitation energies. For guanine-keto−N9-H, different correlated methods have also rendered different vertical excitation energies as shown in Table 4 for comparison.[7]

No minimum energy points on the potential energy surface of the first $\pi-\pi^*$ excited state were found for both tautomers of HPX, however, some stationary points with planar geometries were found in both cases (not shown). Minima on the crossing seam (MXS) for the $\pi-\pi^*/S_0$ CI of HPX-keto-N7-H and HPX-keto-N9-H were found with the algorithm implemented in COLUMBUS for CI search and optimization. The energies for these MXSs are also included in Table 4. The geometries for the MXSs are highly distorted (E_2 in the nomenclature proposed by Boeyens[62]) and resemble the geometries of the CIs found in guanine-keto−N9-H as described in Figure 6. The loss of planarity is due mainly to the out of the plane opposite motion of C2 and N3 (for both HPX and guanine). This can be described quantitatively by the ring puckering parameter, Q, proposed by Cremer and Pople.[63] Some dihedral angles reported for guanine are used to compare the geometric structure of the CIs (keto-N9-H and keto-N7-H) with those which we found for HPX (see legend on Figure 6).

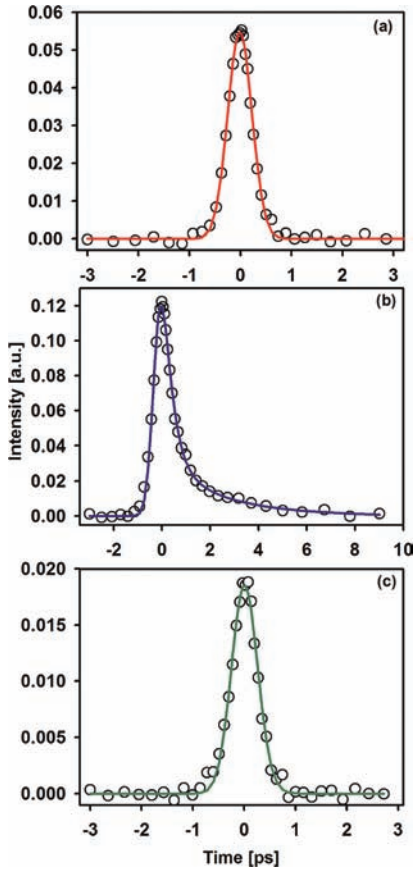

Figure 5. Fluorescence up-conversion measurements of different INS aqueous solutions. (a) pH = 6. (b) INS in HCl 1 N. (c) pH = 10. The excitation and detection wavelength were 257 and 350 nm respectively. The solid lines are nonlinear least-squares fits to exponential decays convoluted with the instrument response function.

Corrected energies at the MRMP2 level for the MXSs calculated at the MRCIS level are shown in Table 4. At the MRMP2 level of theory S_1 and S_0 are not degenerate anymore (ΔE = 0.43 and 0.39 eV for HPX-keto-N9-H and HPX-keto-N7-H, respectively), so that, the reported energies for the conical intersections at the MRMP2 level are taken as the mean value of the energies of S_1 and S_0. These energies are lower than for the S_1 (L_a) state at the FC geometry (S_{0min}) as expected. The small energetic difference between S_1 and S_0 at the MRMP2 level indicates that the CIs calculated at the MRCIS level are near to the CIs that could be predicted at the higher

dx.doi.org/10.1021/ja300546x | J. Am. Chem. Soc. 2012, 134, 7820−7829

Table 4. Vertical Excitation Energies and S_1-S_0 Conical Intersection Energies with Respect to the Optimized S_0 Level for the First $\pi-\pi^*$ State for the Relevant Tautomers of Guanine and Hypoxanthine (HPX)

vertical excitation energies[a] (eV)		
	guanine-keto−N9-H	
MR-CIS[7]	CASPT2[30]	CASPT2[64]
5.82	4.93	4.51
	guanine-keto−N7-H CASPT2	
	4.37[65]	
	HPX-keto−N9-H	
MR-CIS	MRMP2	
5.30	4.48	
	HPX-keto−N7-H	
MR-CIS	MRMP2	
5.88	4.64	

conical intersection energies $\pi-\pi^*$/g.s.[a,b] (eV)		
	guanine-keto−N9-H	
MR-CIS[7]	CASPT2[30]	CASPT2[64]
4.07 (1.75) E_2	4.3 (0.63) ^2E	3.4 (1.11) E_2
	guanine-keto−N7-H CASPT2[65]	
	4.02 (0.35)	
	HPX-keto−N9-H	
MR-CIS	MRMP2	
3.79 (1.51) E_2	3.65 (0.83)	
	HPX-keto−N7-H	
MR-CIS	MRMP2	
3.65 (2.23) E_2	3.58 (1.05)	

[a]Vertical excitation energies and conical intersection energies with respect to the optimized ground state (g.s) energy at the same level of theory. [b]E_2 and ^2E refer to the geometries of the conical intersections according to the Boeyens[62] nomenclature for ring puckering. Values in parentheses are the energies at the Franck−Condon region minus the energy at the conical intersection for the first $\pi-\pi^*$ state (ΔE_{FC-CI})

level of theory MRMP2. S_1 and S_0 states have mainly contributions from the closed shell and HOMO→LUMO configuration state functions at the SA-CASSCF(18,13) level for the MXS geometry found with the MR-CIS methodology.

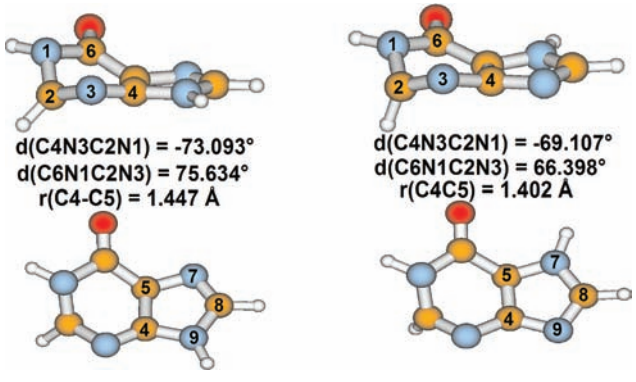

Figure 6. Geometries at the minimum in the crossing seam (MXS) for hypoxanthine-keto−N9-H (left) and hypoxanthine-keto−N7-H (right). (a) For the photophysically relevant conical intersection found by Serrano-Andres et al.[30] in guanine-keto-N9-H these geometrical parameters are r(C4C5) = 1.453 Å and d(C6N1C2N3) = −73.605°. (b) Domcke et al.[64] reported d(C4N3C2N1) = 69° and 72.5°for two conical intersections in guanine-keto-N9-H. (c) Yamazaki and Domcke[65] reported d(C4N3C2N1) = 71° at the geometry of the conical intersection found in guanine-keto-N7-H.

Domcke et al.[64] and Yamasaki et al.[65] have evaluated the accessibility to the $\pi-\pi^*/S_0$ conical intersections by calculating the CASPT2 energies of the $\pi-\pi^*$ and S_0 (g.s) states and using the C4−N3−C2−N1 dihedral angle as the reaction coordinate. In summary, those computations predict that the reaction paths from the Franck−Condon region to the $\pi-\pi^*/S_0$ CI are essentially barrierless for both tautomers of guanine (keto-N9-H and keto-N7-H). Other studies however have shown the existence of plateau regions for the ^1L_a state of this molecule in the solution phase, which explains the near 1 ps component for the excited state decay for the guanine and derived systems (see next section).[13] Since no minima were found in our work for HPX it is also expected that the path from FC to the CI is barrierless.

We have used the relation between the difference between the vertical excitation energy at the FC geometry and the energy of the conical intersection, divided by the ring puckering parameter (Q): $\Delta E_{FC-CI}/Q$, to qualitatively evaluate the accessibility to the CI region in HPX in comparison with guanine. The values for these parameters are included in Tables 4 and 5. As a first approximation, the higher the $\Delta E_{FC-CI}/Q$, the CI is considered to be more accessible, given that this reflects a steeper descent path from the Franck−Condon region to the $\pi-\pi^*$/g.s CI. The specific values in Table 5 should be taken with some reserve given that different methodologies provide slightly different geometries for the CIs and different energies for the vertical excitations and the CIs. However, from our experimental results and the $\Delta E_{FC-CI}/Q$ values calculated for guanine-9H and the HPX tautomers (see Table 5), we can infer that the CIs in HPX-keto−N7-H and HPX-keto−N9-H are highly accessible which explains the ultrafast pathway for the S_1 state in HPX. The experimental difference in the S_1 lifetimes (sub-200 fs versus up to 0.78 ps) show that the HPX and INS systems actually reach the CI region in a significantly faster time scale in comparison with guanine-9H (see below).

Table 5. Ring Puckering Parameter Q (Å) and $\Delta E_{FC-CI}/Q$ (eV/Å) Values for Guanine-keto-N9-H and the Relevant Hypoxanthine Tautomers

Q, ($\Delta E_{FC-CI}/Q$)[a]		
	Guanine-9H	
MR-CIS[7]	CASPT2[30]	CASPT2[64]
0.51 (3.43)	0.61 (1.03)	0.69 (1.61)
	HPX-keto-N9-H	
MR-CIS	MRMP2	
0.62 (2.44)	0.62 (1.33)	
	HPX-keto−N7-H	
MR-CIS	MRMP2	
0.53 (4.21)	0.53 (1.98)	

[a]ΔE_{FC-CI} are the values presented in parentheses in Table 4 and correspond to the energies at the Franck−Condon region minus the energy at the conical intersection for the first $\pi-\pi^*$ state (eV). The $\Delta E_{FC-CI}/Q$ values are presented in parentheses next to the respective Q parameter.

Comparisons with the Guanine Chromophore. Among the most important result of the present study is that the HPX and INS dynamics are different from the case of guanine/guanosine in aqueous solution, where the S_1 population decay shows a biexponential behavior with τ_1 = 0.16 ps and τ_2 = 0.78

ps (2′-deoxyguanosine).[13,59] Calculations at the TD-DFT level of theory that include the effects of the aqueous solvent shell have indicated that this behavior is due to evolution in the excited state surface starting from the Franck−Condon region and the presence of a plateau region in the S_1 surface.[9,13] The faster fluorescence decay in HPX and INS indicates a change in the shape of the S_1 potential energy surface in solution in comparison with guanine. The change is likely to be related to a steeper gradient leading to the CI, which would result in significantly shorter fluorescence lifetimes. This difference is necessarily associated to the lack of the amino group at position C2 which can change the potential energy surface in the region of the reaction coordinate in the solution phase. The changes in the solution phase dynamics with respect to guanine could also be specifically related to a reduced capacity to form hydrogen bonds with the solvent.

The gas phase ultrafast excited state conversion of guanine shows a two exponential decay in 0.148 and 0.36 ps (molecular beams, pump−probe resonant ionization[66]), and has been the subject of several interpretations based on computational results.[8,30,64,67,68] Serrano Andres et al. proposed a three state model from minimum energy paths. From those calculations, the faster time constant in the gas phase was associated to the crossing through a conical intersection due to the puckering of the C2 carbon.[30] The longer decay time of 0.36 ps was suggested to be due to participation of an n−π^* state. On the other hand, nonadiabatic dynamics for excited guanine have been performed with potential energy surfaces computed by Restricted Open Shell Kohn−Sham methods (ROKS by Langer et al.),[69] semi empirical methods (OM2-MRCI by Lan et al.),[8] and most recently, extended ab initio methods based on the MR-CI method, with on-the-fly surface hopping dynamics (MR-CIS by Barbatti et al.).[7]

The two most recent simulations of the gas phase dynamics for guanine[7,8] have shown that the deactivation process actually occurs nearly exclusively from the first π−π^* state (S_1−S_0 process). However, these calculations do not predict the participation of the exact same set of conical intersections: the OM2-MRCI method determines the existence of an S_1 decay channel associated to a CI with a pronounced out of plane displacement of the C2 atom (ethylenic II type according to ref 7.). The OM2-MRCI method also determines the existence of a second type of pathway that directs the system to another CI, this one associated with an out-of-plane distortion of the amino group with a strong C2−N3 stretching and puckering at C5 and C6.

The MR-CIS calculations of Barbatti et al. have shown again the major participation of two types of conformations for the S_1 deactivation. In this case, both of them with significantly puckered C2 atoms (named ethylenic I and ethylenic II CIs[7]). One of the CIs of the MR-CIS dynamics calculations of ref 7 coincides with the first intersection mentioned above for the OM2-MRCI method (ethylenic II, also coincident with ref 30). However, the MR-CIS calculations do not predict the presence of the second intersection observed by the OM2-MRCI method, but instead, calculates a so-called ethylenic I type intersection (E_2) where the C2 atom is also puckered (as in the ethylenic II CI), but now, with the amino group at about 80° to 90° with respect to the ring system (see Figure 2 in ref 7).

The present measurements on the HPX and INS systems are conclusive in regards to the fact that the $-NH_2$ group is not essential for the ultrafast decay of the π−π^* state, and that the dynamics are much faster than for guanine/guanosine in aqueous solution. We believe that thanks to the present experimental results, the HPX chromophore can serve as a crucial case-study in calculations and dynamics simulations to fully understand the fundamental aspects of the electronic deactivation in purines. Our experimental results indicate that the CIs we calculated, which are also due to the C2 atom puckering, are reached more directly in the HPX systems. The characterization of this similar but simpler purine should also test for the participation of the other CIs, and overall, contribute to define which is the appropriate level of theory to predict the observed behavior.

Photophysics of Singly Protonated Hypoxanthine and Inosine. At pH = 1, monoprotonated (**2**, HPX^+) and neutral (**1a** + **1b**) HPX exist in relative concentrations of 92% and 8% respectively, while in a 1 N HCl solution, the monoprotonated population is estimated to approach 99%. This is concluded from population diagrams as a function of pH built from the reported pK_a values.[39,44] The results of the up-conversion experiments for the pH = 1 sample are shown in Figure 4b. Differently from the neutral solutions, the low pH solutions show a biexpoenential decay with τ_1 < 0.2 ps and τ_2 = 1.1 ps, where this last component is related to about 5% of the total signal amplitude. This result is similar for the 1 N HCl HPX solutions τ_1 < 0.2 ps and τ_2 = 1.1 ps (data not shown). We ascribe the first term (τ_1 < 0.2 ps in pH = 1) to the early evolution of the S_1 state for HPX^+, including population decay and some wave packet evolution from the Franck−Condon region in the $S_1(\pi$−$\pi^*)$ state (a small fraction of the ultrafast signal could also come from the small fraction (8%) of neutral molecules at this pH). Given the presence of a second component of 1.1 ps, some population branching probably takes place so that the deactivation of a fraction of the S_1 population appears to take place after the initial evolution, giving rise to the 1.1 ps (notice that the ^1L_a and the ^1L_b states have a smaller gap which could be a related effect).

For INS in HCl 1 N, according to the reported pK_a values,[39,40] the predominant specie is monoprotonated INS (**5**) at a mole fraction of 90% (the rest corresponding to neutral INS). Monoprotonated HPX (**2**) and monoprotonated INS (**5**) show similar biexponential decays (with τ_1 = 0.39 ps and τ_2 = 2.5 ps for INS^+, see Table 3 and Figure 5b). This is actually expected since the protonated purinic heterocycle has analogous structures in **2** and **5**. That is, in both cases the protonation site is N7, and the formal positive charge is delocalized through the π system. A biexponential behavior has been observed in the parent system, singly protonated guanine. However, monoprotonated guanine, monoprotonated guanosine and $GMPH^+$ have much longer fluorescence lifetimes of up to 196 ps.[13,14] From these results we can conclude that the removal of the amino group (absent in HPX^+ and INS^+) again redounds in important differences in the photophysics, making the S_1 lifetimes much shorter in HPX^+ and in INS^+ in comparison with the monoprotonated forms of guanine/guanosine. In the monoprotonated guanine systems, the internal reaction coordinate responsible of the slow S_1 deactivation (e.g., 196 ps lifetime for guanosine, pH = 1, ref 14) has been determined to be an opposite out of plane motion of the H atoms bond at C8 and N7.[13] Our results indicate that the lack of the amino group in these monoprotonated forms reduces the lifetimes drastically, implying significant changes in the potential energy surfaces due to the alteration in the substitution pattern in the six member ring (absence of the $-NH_2$ group). In pyrimidine bases the amino group has also

dx.doi.org/10.1021/ja300546x | J. Am. Chem. Soc. 2012, 134, 7820−7829

been found to be very important in the fluorescence behavior of the bases. For example, removal of the amino group in cytosine makes the lifetimes of the excited state longer.[35]

Photophysics of Singly Deprotonated Hypoxanthine and Inosine. For the studies of the conjugated bases of hypoxanthine and inosine, the solution was adjusted to have a pH = 10, since in this condition the population of the singly deprotonated form is maximal in comparison with the neutral species, while the doubly deprotonated form remains at a minimal concentration (< 7% for HPX and < 6% for INS).[39,44] The up-conversion traces for HPX at pH = 10 show a biexponential fluorescence decay with τ_1 < 0.2 ps (60%) and τ_2 = 19.0 ps (40%), see Figure 4c. In these conditions, the neutral forms of HPX (**1a**/**1b**) correspond to about 7% of the population, which is enough to contribute to the ultrafast component of the 350 nm fluorescence decay. However, if the biexponential behavior was only due to the presence of different species with different lifetimes (τ_1 and τ_2), the pre-exponential factors would render the relative concentrations of the two species (this, assuming similar absorption coefficients and radiative rates). Supposing that neutral and singly deprotonated hypoxanthine (HPX^-) are responsible for the τ_1 and τ_2 components respectively, the relative concentration of deprotonated HPX (**3**) would be approximately: $a_1/(a_1 + a_2)$ = 0.4 (see Table 3, note that the signals are convoluted and therefore, the plots do not directly reflect the exponential amplitudes). This value appears too low to represent the population of the singly deprotonated form since the HPX^- population at pH 10 is 86% (pK_{a_2} = 8.6). Therefore, it is most likely that the biexponential behavior is intrinsic of the deprotonated form, and that the early component might be related to the evolution from the Franck–Condon region with some contribution from the neutral species (which have ultrafast decays). The presence of a 19 ps component is a remarkable feature of this study, since it reflects an important change in the shape of the emissive state surface upon the removal of a single proton, leaving the five membered ring's nitrogens, N7 and N9 atoms in their deprotonated state (see **3** in Figure 1). Furthermore, the effect which produces this time component could also be related with the presence of n–π^* states near the optically accessed L_a (π–π^*) singlet state at the FC geometry (see Table 1).

Most interesting of the monodeprotonated forms is that HPX^- (**3**) and INS^- (**6**) actually have completely different excited state decays. This can be seen in Figure 5c which shows that INS^- maintains the single exponential ultrafast fluorescence decay of INS (τ < 0.2 ps), which is 2 orders of magnitude shorter than the HPX^- fluorescence lifetime (τ_2 = 19 ps, see Figure 4c). Such large difference in the photophysics can be related directly to differences in the chemical structures of these two basic forms: while in HPX^- position N1 is protonated and positions N7 and N9 are deprotonated, in INS^-, N9 is ribose-substituted while N1 is deprotonated (see **6** in Figure 1). These results make it clear that different deprotonation sites produce contrasting effects in the excited state evolution. Interestingly, the deactivation of the excited state is slower in monoanionic HPX, where deprotonation occurs in the pirazole ring, which is involved in the tautomerism of neutral aqueous HPX. Considering that similarly to guanine, the loss of planarity in the pyrimidinic ring is most likely responsible for the evolution in the first π–π^* excited state surface,[13] the deprotonation in HPX appears to have a long-range effect on this puckering coordinate of the emissive state potential energy surface, while in INS^- (N1 deprotonation), the ultrafast decay is unaffected, corresponding to a similar surface to that of the neutral form. Theoretical calculations of the CIs in the ionized forms and studies about the accessibility to the crossing seams will be presented in an upcoming contribution.

■ CONCLUSIONS

The hypoxanthine heterocyclic system shows very interesting variations in its photophysics in comparison with other purines. The main tautomers at near neutral pH, keto–N7-H and keto–N9-H, and the nucleoside INS have ultrafast S_1 decay channels which are as fast as the natural base adenine, and much faster than the parent compound guanine. This can be related directly to the lack of the amino group at position C2 of guanine. Our results can be already interpreted as an effect of having a more simple six membered cycle in HPX (without the $-NH_2$ substitution), which reaches the S_1–S_0 CI through a loss of planarity with a C2 pyramidalization (see Figure 6). The CI is highly accessible and this is related to a faster excited state decay in HPX than in guanine.[13,30] Furthermore, the presence of the NH_2 group in guanine at the C2 position, as opposed to a hydrogen in HPX, may have kinematic effects on the motion along this coordinate.[70]

Single protonation of HPX only produces a somewhat slower fluorescence decay in comparison with the neutral tautomers, with an extra 1.1 ps component (5%). This is in contrast with the parent guanine system where protonation is associated with a much larger increase in the S_1 lifetimes (196 ps for guanosineH^+), such difference again is likely to be related to the absence of the amino group which greatly increases the accessibility to the S_1–S_0 CI in the HPX^+ system as well.

Deprotonation of HPX has an important effect, making the emissive state have a long lifetime of 19 ps, 2 orders of magnitude slower than the neutral forms. This slower decay is due to the lack of protons at both N7 and N9, leaving only one H-substituted site at N1. The monoanion of INS on the other hand, keeps the sub 0.2 ps decay of the first π–π^* state and does not show a long 19 ps component. Such differences between HPX^- and INS^- can be associated directly to the fact that deprotonation of INS produces a completely different electron distribution given that this system is deprotonated at N1 and ribose-substituted at N9 as seen in Figure 1.

■ AUTHOR INFORMATION

Corresponding Author

jpeon@servidor.unam.mx

Notes

The authors declare no competing financial interest.

■ ACKNOWLEDGMENTS

For financial support, we are thankful to Consejo Nacional de Ciencia y Tecnología (CONACyT, Grant 79494), and to Universidad Nacional Autónoma de México (PAPIIT, Grant IN212907). We thank DGTIC for some of the computational resources. SM acknowledges support from the National Science Foundation under grant CHE 0911474.

■ REFERENCES

(1) Pecourt, J. M. L.; Peon, J.; Kohler, B. *J. Am. Chem. Soc.* **2001**, *123*, 10370–10378.

(2) Middleton, C. T.; de La Harpe, K.; Su, C.; Law, Y. K.; Crespo-Hernandez, C. E.; Kohler, B. *Annu. Rev. Phys. Chem.* **2009**, *60*, 217−239.
(3) Crespo-Hernandez, C. E.; Cohen, B.; Hare, P. M.; Kohler, B. *Chem. Rev.* **2004**, *104*, 1977−2019.
(4) Peon, J.; Zewail, A. H. *Chem. Phys. Lett.* **2001**, *348*, 255−262.
(5) Serrano-Andres, L.; Merchan, M. *J.Photochem. Photobiol., C: Photochem. Rev.* **2009**, *10*, 21−32.
(6) Barbatti, M.; Lischka, H. *J. Am. Chem. Soc.* **2008**, *130*, 6831−6839.
(7) Barbatti, M.; Szymczak, J. J.; Aquino, A. J. A.; Nachtigallova, D.; Lischka, H. *J. Chem. Phys.* **2011**, *134*, 014304.
(8) Lan, Z. G.; Fabiano, E.; Thiel, W. *ChemPhysChem* **2009**, *10*, 1225−1229.
(9) Gustavsson, T.; Improta, R.; Markovitsi, D. *J. Phys. Chem. Lett.* **2010**, *1*, 2025−2030.
(10) Morales-Cueto, R.; Esquivelzeta-Rabell, M.; Saucedo-Zugazagoitia, J.; Peon, J. *J. Phys. Chem. A* **2007**, *111*, 552−557.
(11) Zgierski, M. Z.; Fujiwara, T.; Lim, E. C. *Chem. Phys. Lett.* **2008**, *463*, 289−299.
(12) Hassan, W. M. I.; Chung, W. C.; Shimakura, N.; Koseki, S.; Kono, H.; Fujimura, Y. *Phys. Chem. Chem. Phys.* **2010**, *12*, 5317−5328.
(13) Karunakaran, V.; Kleinermanns, K.; Improta, R.; Kovalenko, S. A. *J. Am. Chem. Soc.* **2009**, *131*, 5839−5850.
(14) Fujiwara, T.; Kamoshida, Y.; Morita, R.; Yamashita, M. *J. Photochem. Photobiol. B Biol.* **1997**, *41*, 114−121.
(15) Nolting, D.; Weinkauf, R.; Hertel, I. V.; Schultz, T. *ChemPhysChem* **2007**, *8*, 751−755.
(16) Marian, C.; Nolting, D.; Weinkauf, R. *Phys. Chem. Chem. Phys.* **2005**, *7*, 3306−3316.
(17) Plaza-Medina, E. F.; Rodriguez-Cordoba, W.; Morales-Cueto, R.; Peon, J. *J. Phys. Chem. A* **2011**, *115*, 577−585.
(18) Plaza-Medina, E. F.; Rodriguez-Cordoba, W.; Peon, J. *J. Phys. Chem. A* **2011**, *115*, 9782−9789.
(19) Boens, N.; Qin, W.; Basarić, N.; Hofkens, J.; Ameloot, M.; Pouget, J.; Lefèvre, J.-P.; Valeur, B.; Gratton, E.; vandeVen, M.; Silva, N. D.; Engelborghs, Y.; Willaert, K.; Sillen, A.; Rumbles, G.; Phillips, D.; Visser, A. J. W. G.; van Hoek, A.; Lakowicz, J. R.; Malak, H.; Gryczynski, I.; Szabo, A. G.; Krajcarski, D. T.; Tamai, N.; Miura, A. *Anal. Chem.* **2007**, *79*, 2137−2149.
(20) Schweize, Mp; Broom, A. D.; Tso, P. O. P.; Hollis, D. P. *J. Am. Chem. Soc.* **1968**, *90*, 1042−1055.
(21) Nakano, N. I.; Igarashi, S. J. *Biochemistry* **1970**, *9*, 577−583.
(22) Morcillo, J.; Gallego, E.; Peral, F. *J. Mol. Struct.* **1987**, *157*, 353−369.
(23) Martel, P. *J. Phys. Chem.* **1985**, *89*, 230−234.
(24) Hupp, T.; Sturm, C.; Janke, E. M. B.; Cabre, M. P.; Weisz, K.; Engels, B. *J. Phys. Chem. A* **2005**, *109*, 1703−1712.
(25) Haupl, T.; Windolph, C.; Jochum, T.; Brede, O.; Hermann, R. *Chem. Phys. Lett.* **1997**, *280*, 520−524.
(26) Hirao, K. *Chem. Phys. Lett.* **1992**, *190*, 374−380.
(27) Nakano, H. *J. Chem. Phys.* **1993**, *99*, 7983−7992.
(28) Mburu, E.; Matsika, S. *J. Phys. Chem. A* **2008**, *112*, 12485−12491.
(29) Perun, S.; Sobolewski, A. L.; Domcke, W. *J. Am. Chem. Soc.* **2005**, *127*, 6257−6265.
(30) Serrano-Andres, L.; Merchan, M.; Borin, A. C. *J. Am. Chem. Soc.* **2008**, *130*, 2473−2484.
(31) Schmidt, M. W.; Baldridge, K. K.; Boatz, J. A.; Elbert, S. T.; Gordon, M. S.; Jensen, J. H.; Koseki, S.; Matsunaga, N.; Nguyen, K. A.; Su, S.; Windus, T. L.; Dupuis, M.; Montgomery, J. A. *J. Comput. Chem.* **1993**, *14*, 1347−1363.
(32) Bode, B. M.; Gordon, M. S. *J. Mol. Graphics Modell.* **1998**, *16*, 133−138.
(33) Lischka, H.; Müller, T.; Szalay, P. G.; Shavitt, I.; Pitzer, R. M.; Shepard, R. *Wiley Interdiscip. Rev.: Comput. Mol. Sci.* **2011**, *1*, 191−199.
(34) Dallos, M.; Lischka, H.; Shepard, R.; Yarkony, D. R.; Szalay, P. G. *J. Chem. Phys.* **2004**, *120*, 7330−7339.
(35) Kistler, K. A.; Matsika, S. *J. Phys. Chem. A* **2007**, *111*, 2650−2661.
(36) Matsika, S. *J. Phys. Chem. A* **2004**, *108*, 7584−7590.
(37) Barbatti, M.; Aquino, A. J. A.; Szymczak, J. J.; Nachtigallová, D.; Hobza, P.; Lischka, H. *Proc. Natl. Acad. Sci. U.S.A.* **2010**, *107*, 21453−21458.
(38) Linder, P. W.; Stanford, M. J.; Williams, D. R. *J. Inor. Nucl. Chem.* **1976**, *38*, 1847−1849.
(39) Izatt, R. M.; Jj, Christen.; Rytting, J. H. *Chem. Rev.* **1971**, *71*, 439−481.
(40) Tauler, R.; Cid, J. F.; Casassas, E. *J. Inorg. Biochem.* **1990**, *39*, 277−285.
(41) Medeiros, G. C.; Thomas, G. J. *Biochim. Biophys. Acta* **1971**, *238*, 1−4.
(42) Psoda, A.; Shugar, D. *Biochim. Biophys. Acta* **1971**, *247*, 507−513.
(43) Sun, X. J.; Lee, J. K. *J. Org. Chem.* **2007**, *72*, 6548−6555.
(44) Benoit, R. L.; Frechette, M. *Can. J. Chem.* **1985**, *63*, 3053−3056.
(45) Clark, L. B.; Tinoco, I. *J. Am. Chem. Soc.* **1965**, *87*, 11−15.
(46) Lichtenb., D; Neiman, Z.; Bergmann, F. *Isr. J. Chem.* **1972**, *10*, 805−817.
(47) Chenon, M. T.; Pugmire, R. J.; Grant, D. M.; Panzica, R. P.; Townsend, L. B. *J. Am. Chem. Soc.* **1975**, *97*, 4636−4642.
(48) Kondratyuk, I. V.; Samijlenko, S. P.; Kolomiets, I. M.; Hovorun, D. M. *J. Mol. Struct.* **2000**, *523*, 109−118.
(49) Shukla, M. K.; Leszczynski, J. *Int. J. Quantum Chem.* **2005**, *105*, 387−395.
(50) Fernandez-Quejo, M.; de la Fuente, A.; Navarro, R. *J. Mol. Struct.* **2005**, *744*, 749−757.
(51) Gogia, S.; Jain, A.; Puranik, M. *J. Phys. Chem. B* **2009**, *113*, 15101−15118.
(52) Costas, M. E.; AcevedoChavez, R. *J. Phys. Chem. A* **1997**, *101*, 8309−8318.
(53) Roman-Zimbron, M. L. S.; Costas, M. E.; Acevedo-Chavez, R. *J. Mol. Struct:Theochem* **2004**, *711*, 83−94.
(54) Bartl, T.; Zacharova, Z.; Seckarova, P.; Kolehmainen, E.; Marek, R. *Eur. J. Org. Chem.* **2009**, *2009*, 1377−1383.
(55) Voelter, W.; Records, R.; Bunnenberg, E.; Djerassi, C. *J. Am. Chem. Soc.* **1968**, *90*, 6163−6170.
(56) Shukla, M. K.; Leszczynski, J. *J. Phys. Chem. A* **2003**, *107*, 5538−5543.
(57) Ludwig, V.; da Costa, Z. M.; do Amaral, M. S.; Borin, A. C.; Canuto, S.; Serrano-Andrés, L. *Chem. Phys. Lett.* **2010**, *492*, 164−169.
(58) Klenwächter, V.; Drobnik, J.; Augenstein, L. *Photochem. Photobiol.* **1967**, *6*, 133−146.
(59) Onidas, D.; Markovitsi, D.; Marguet, S.; Sharonov, A.; Gustavsson, T. *J. Phys. Chem. B* **2002**, *106*, 11367−11374.
(60) Röttger, K.; Temps, F. In; *The Madrid Conference on Femtochemistry* FEMTO10, Madrid, Spain, 2011; p 227.
(61) Cohen, B.; Hare, P. M.; Kohler, B. *J. Am. Chem. Soc.* **2003**, *125*, 13594−13601.
(62) Boeyens, J. C. A. *J. Chem. Crystallogr.* **1978**, *8*, 317−320.
(63) Cremer, D.; Pople, J. A. *J. Am. Chem. Soc.* **1975**, *97*, 1354−1358.
(64) Yamazaki, S.; Domcke, W.; Sobolewski, A. L. *J. Phys. Chem. A* **2008**, *112*, 11965−11968.
(65) Yamazaki, S.; Domcke, W. *J. Phys. Chem. A* **2008**, *112*, 7090−7097.
(66) Canuel, C.; Mons, M.; Piuzzi, F.; Tardivel, B.; Dimicoli, I.; Elhanine, M. *J. Chem. Phys.* **2005**, *122*, 074316.
(67) Chen, H.; Li, S. H. *J. Chem. Phys.* **2006**, *124*, 154315.
(68) Marian, C. M. *J. Phys. Chem. A* **2007**, *111*, 1545−1553.
(69) Langer, H.; Doltsinis, N. L. *Phys. Chem. Chem. Phys.* **2004**, *6*, 2742−2748.
(70) Hudock, H. R.; Levine, B. G.; Thompson, A. L.; Satzger, H.; Townsend, D.; Gador, N.; Ullrich, S.; Stolow, A.; Martínez, T. J. *J. Phys. Chem. A* **2007**, *111*, 8500−8508.